Research Square

Preprints are preliminary reports that have not undergone peer review.
They should not be considered conclusive, used to inform clinical practice,
or referenced by the media as validated information.

Thalamic volume links milder symptoms but faster dopaminergic decline in prodromal Parkinson disease

Zhicong Wang
The First Affiliated Hospital of Xiamen University, School of Medicine, Xiamen University
Liqing Xie
Children's Hospital of Fudan University Xiamen Branch
Jingjing Wu
University of Bonn
Chengfeng Wang
University of Bonn
Ruiqing Ni
ruiqing.ni@unibe.ch
Inselspital University of Bern
Jianhua Wang
The First Affiliated Hospital of Xiamen University, School of Medicine, Xiamen University

Research Article

Keywords:

Posted Date: September 30th, 2026

DOI: https://doi.org/10.21203/rs.3.rs-11083698/v1

License: This work is licensed under a Creative Commons Attribution 4.0 International License.
Read Full License

Additional Declarations: No competing interests reported.

Thalamic volume links milder symptoms but faster dopaminergic decline in prodromal Parkinson disease

Zhicong Wang[1,2,3], Liqing Xie[4,3], Jingjing Wu[3,5], Chengfeng Wang[3], Ruiqing Ni[*6], and Jianhua Wang[*1,2]

[1]Department of Radiology, The First Affiliated Hospital of Xiamen University, School of Medicine, Xiamen University, Xiamen, China
[2]Xiamen First Clinical Medical College of Fujian Medical University, Xiamen, China
[3]Medical Faculty, University of Bonn, Bonn, Germany
[4]Department of Child Healthcare, Children's Hospital of Fudan University (Xiamen Branch), Xiamen, China
[5]Department of Neurology, The Affiliated Hospital of Xuzhou Medical University, Xuzhou, Jiangsu, China
[6]Department of Nuclear Medicine, Inselspital University of Bern, 3010 Bern, Switzerland
[*]Co-corresponding authors: Ruiqing Ni (ruiqing.ni@unibe.ch); Jianhua Wang (wangjianhua@xmu.edu.cn)

Abstract

Background: Biological changes such as α-synuclein deposits and brain structural changes related to Parkinson's disease (PD) may precede both clinical diagnosis and dopaminergic dysfunction. However, whether magnetic resonance imaging (MRI)-derived structural features are associated with clinical burden and can predict subsequent dopaminergic changes remains unclear.
Purpose: To determine whether multilevel baseline MRI phenotypes are associated with concurrent clinical status (including motor severity, overall disease stage, and global cognitive performance) and longitudinal changes in the dopamine transporter (DAT) ratio, to localize the anatomical regions involved.
Materials and Methods: In this longitudinal cohort study, we analysed T1-weighted MRI from 340 participants from the PPMI who were cerebrospinal fluid α-synuclein seed amplification assay (SAA)-positive, DAT-negative and without a clinical diagnosis of PD at baseline. Longitudinal mixed-effects models sequentially evaluated four broad MRI summary measures, seven prespecified regional measures and 25 thalamic nuclei. We assessed the link between MRI measures with motor severity, disease stage and cognition in the PPMI chohrt, and independently assessed in the Quebec Parkinson Network Neuroimaging Cohort.
Results: None of the four broad MRI summary measures were associated with longitudinal changes in the DAT. Baseline thalamic volume was associated with an additional decrease in the annual DAT ratio of 0.018 ($\beta = -0.018$, 95% CI, $[-0.031, -0.005]$; $FDR = 0.046$). Nucleus-level analysis revealed five FDR-significant nuclei in the basal ganglia–thalamocortical loops. In the primary cohort, the five-nucleus composite was associated with lower Movement Disorder Society Unified Parkinson's Disease Rating Scale Part III (UPDRS-III) scores ($\beta = -0.790$, $FDR = 0.022$). In the independent Quebec PD cohort, greater thalamic volume was associated with lower UPDRS-III scores ($\beta = -4.382$, $FDR = 0.040$), lower Hoehn–Yahr stages ($OR = 0.320$, $FDR < 0.001$) and higher Montreal Cognitive Assessment (MoCA) scores ($\beta = 1.709$, $FDR = 0.002$).
Conclusion: Thalamic structure was selectively associated with subsequent decreases in the DAT among patients with broad baseline MRI phenotypes. Despite its association with faster subsequent DAT decline, the concurrent association of greater thalamic structure with milder clinical involvement indicates that the brain structure, current clinical state and subsequent dopaminergic dysfunction may not evolve synchronously during early PD.

Introduction

Parkinson's disease (PD) is the second most common progressive neurodegenerative disorder worldwide and is characterized by bradykinesia, rest tremor and rigidity, together with a broad range of non-motor manifestations[1;2]. Although PD continues to be diagnosed primarily on the basis of a characteristic motor syndrome, its underlying biological processes may begin many years before clinical diagnosis[3–5]. Recently proposed biological staging frameworks further emphasize that pathological α-synuclein aggregation and nigrostriatal dopaminergic dysfunction may emerge at different stages of the disease rather than when detectable abnormalities are reached simultaneously[6]. Cerebrospinal fluid α-synuclein seed amplification assays (SAA) can detect pathological α-synuclein seeding activity, whereas dopamine transporter (DAT) single-photon emission computed tomography (SPECT) imaging provides a complementary measure of presynaptic nigrostriatal dopaminergic terminal integrity[6–8]. Individuals who are SAA positive but whose standardized lowest-putamen DAT ratio remains above the prespecified abnormality threshold therefore have molecular evidence of α-synuclein pathology without conventional DAT-SPECT scans abnormalities. Because the DAT-negative status is defined by a threshold, it does not exclude interindividual variation or gradual longitudinal change above that threshold. This biomarker combination consequently defines a pathologically enriched early research window in which to test whether baseline brain structure is associated with subsequent dopaminergic changes.

Structural magnetic resonance imaging (MRI) provides anatomical information complementary to the molecular pathology indexed by SAA and the dopaminergic function indexed by DAT-SPECT scan. Dopaminergic dysfunction in PD is not confined to a single region but involves distributed neural networks linking the basal ganglia, thalamus, cerebellum and cerebral cortex[9–11]. Early structural differences associated with subsequent dopaminergic dysfunction may therefore appear either as broad variation shared across multiple regions or as more spatially concentrated differences within specific anatomical structures. Previous structural and diffusion MRI studies have identified cross-sectional differences and longitudinal changes in the brain of patients with clinically diagnosed or de novo PD, and have related some of these changes to motor phenotypes and disease progression[12–15]. However, these studies have generally focused on diagnostic-group differences, concurrent clinical manifestations or changes in brain structure itself. Whether baseline MRI structure is associated with subsequent continuous DAT trajectories before conventional DAT imaging reaches the threshold for abnormality remains unclear. Addressing this question also requires distinguishing structural information expressed at different spatial scales. Broad MRI summary measures can capture structural variation shared across regions, whereas regional morphometric measures can localize more anatomically concentrated associations. It therefore remains unknown whether baseline MR images contain structural information related to subsequent dopaminergic changes and whether such information is expressed primarily at a broad or region-specific anatomical level.

Within these distributed networks, the thalamus occupies a particularly important system-level position. It participates in both basal ganglia–thalamo–cortical and cerebello–thalamo–cortical circuits, relaying and integrating signals from the basal ganglia and cerebellum across motor, associative and limbic cortical territories, thereby contributing to motor control, cognitive processing and affective regulation[9–11;16]. Dopaminergic dysfunction may therefore not only alter thalamic activity through changes in basal ganglia output but also be accompanied by reorganization of neural activity, synchronization and connectivity across thalamocortical networks. Whole-thalamus morphology may integrate structural variation distributed across multiple motor and associative circuits, providing a systems-level anatomical phenotype. Previous structural, diffusion and functional MRI studies have identified alterations of the thalamus and its connected pathways across different stages of PD, although findings vary with disease stage, motor phenotype, imaging method and scanner composition[13;15;17–19]. Moreover, most existing evidence has been obtained from individuals with clinically diagnosed PD; therefore, whether the whole-thalamus structure is associated with subsequent dopaminergic change before conventional

DAT imaging becomes abnormal has not been established. Whole-thalamus morphology consequently provides a biologically grounded candidate for testing system-level links between early brain structure and subsequent DAT trajectories.

However, the thalamus is not a functionally homogeneous anatomical structure. Its constituent nuclei have relatively distinct patterns of cortical, striatal, cerebellar and brainstem connectivity and contribute to motor, associative, limbic and arousal-related functions[10;20]. A systems-level difference reflected by whole-thalamus volume may therefore be distributed across multiple nuclei or concentrated within nuclei with particular connectivity profiles. Modern probabilistic atlases and automated segmentation methods can estimate thalamic nucleus volumes from conventional T1-weighted MRI, providing a feasible approach for resolving this spatial heterogeneity[20–22]. However, existing nucleus-level studies have primarily examined cross-sectional group differences or concurrent symptom associations in patients clinically diagnosed PD, with limited evidence linking baseline nucleus structure to subsequent dopaminergic changes[15;23]. Moreover, nucleus volumes can be strongly correlated with one another and with whole-thalamus volume, potentially causing broadly distributed structural variation to appear anatomically focal on a single screen. Automated segmentation of small nuclei and the use of predefined atlas boundaries may further influence anatomical localization. Thalamus-related networks may also extend into adjacent diencephalic and basal ganglia structures beyond conventional thalamic boundaries. Interpreting any thalamic association therefore requires evaluation at both the whole-thalamus and nucleus levels, explicit control of multiple comparisons, and resampling and expanded-region analyses that distinguish a stable effect direction from the selection of specific nuclei and their anatomical boundaries.

To address these questions, we integrated baseline MRI with longitudinal DAT imaging in participants from the Parkinson's Progression Markers Initiative (PPMI) who were α-synuclein SAA positive, DAT negative and free of a clinical PD diagnosis at baseline[24]. We first compared broad MRI summary measures with prespecified regional morphometric measures to determine the spatial scale at which structural information was associated with subsequent continuous DAT change. We then characterized the thalamic signal identified by this screening across the whole thalamus, 25 thalamic nuclei, an expanded set of subcortical regions and several structural composite scores, and assessed its stability using resampling and site-grouped cross-fitting. Finally, we examined the relationships between the same thalamic measures and clinical status at the time of MRI and validated this clinical association in the independent Quebec Parkinson Network Neuroimaging Cohort (QPN-NC)[25;26]. Broad MRI phenotypes showed no longitudinal associations, whereas larger thalamic structures were associated with faster subsequent DAT decline, with the signal distributed across multiple thalamic nuclei and extending to the VentralDC. Moreover, larger thalamic structures were associated with milder concurrent clinical impairment in both cohorts. By linking multiscale brain structure, current clinical status and subsequent dopaminergic dysfunction, these findings suggest that these dimensions may not evolve in parallel during the early stages of PD.

Results

PPMI cohort and longitudinal DAT-SPECT scan follow-up

The initial PPMI cohort we used included 361 participants, all of whom were SAA-positive, DAT-SPECT scans negative and had not been clinically diagnosed with PD at baseline. Of these, 341 had baseline morphometric data that passed quality control. One participant lacked a calculable post-MRI DAT ratio, leaving 340 participants and 520 post-MRI DAT SPECT points data in the primary longitudinal analysis (Fig. 1a). The analytical sample had a mean age of 68.70 years (s.d., 5.81), included 196 male and 144 female participants, and represented 33 acquisition sites. Additional demographic and baseline clinical characteristics are summarized in Table 1.

Table 1: Baseline characteristics and longitudinal follow-up of the PPMI SAA$^+$/DAT$^-$ cohort

Characteristic	Available n	Summary
Cohort definition		
Participants in the primary longitudinal analysis	–	340
Cerebrospinal fluid SAA-positive	340	340 (100%)
DAT-negative at baseline	340	340 (100%)
No clinical PD diagnosis at baseline	340	340 (100%)
Acquisition sites	340	33
Demographic and baseline clinical characteristics		
Age, years	340	68.70 (5.81)
Sex, male/female	340	196 (57.6%)/144 (42.4%)
RBD phenotype	340	116 (34.1%)
MDS-UPDRS-III score	334	3 [1–6]
Observed range	334	0–35
Standardized lowest-putamen DAT ratio	340	0.827 [0.752–0.922]
Observed range	340	0.650–1.537
Temporal alignment of baseline assessments		
Absolute MRI–baseline DAT-SPECT interval, days	340	91 [60–130]
Absolute MRI–SAA sampling interval, days	340	16 [8–23]
Longitudinal DAT follow-up		
Post-MRI DAT-SPECT	340	520
Participants with 1/2/3 post-MRI DAT-SPECT	340	164/172/4
Time from baseline DAT-SPECT scan, years	520	1.42 [1.25–2.25]
Maximum follow-up per participant, years	340	2.08 [1.33–2.33]
Longest observed follow-up, years	340	4.25

Data are presented as the mean (s.d.), median [interquartile range], range, or n (%), as appropriate. Available n denotes the number of participants with nonmissing data, except for the observation-level follow-up interval. Post-MRI DAT observations were acquired after both baseline MRI and baseline DAT imaging. DAT, dopamine transporter; SPECT, single-photon emission computed tomography; MDS-UPDRS-III, Movement Disorder Society Unified Parkinson's Disease Rating Scale Part III; PD, Parkinson's disease; RBD, rapid eye movement sleep behavior disorder; SAA, α-synuclein seed amplification assay.

All DAT SPECT imaging data included in the longitudinal models were acquired after both baseline MRI and baseline DAT SPECT imaging. Baseline MRI was performed within 180 days before or after baseline DAT, with a median absolute interval of 91 days (interquartile range (IQR), 60–130 days). The median absolute interval between baseline MRI and SAA sampling was 16 days (IQR, 8–23 days). Across all follow-up scans, the median time from baseline DAT SPECT was 1.42 years (IQR, 1.25–2.25 years). The median maximum follow-up per participant was 2.08 years (IQR, 1.33–2.33 years), and the longest observed follow-up was 4.25 years (Fig. 1b).

The primary longitudinal outcome was the continuous standardized lowest-putamen DAT ratio measured at each post-MRI follow-up. Associations with longitudinal changes in the DAT were tested using maximum-likelihood random-intercept linear mixed-effects models. The interaction between time and each baseline imaging measure quantified the difference in the change in the annual DAT ratio associated with a 1-s.d. higher imaging measure. The models included baseline DAT, age, sex and rapid eye movement sleep behavior disorder, together with the interaction of each covariate with time (Fig. 1c).

Baseline thalamic volume corresponded to faster subsequent DAT decline

We first examined four baseline MRI summary measures capturing different levels of brain structure: substantia nigra/ventral tegmental area neuromelanin-sensitive signals, asymmetry, cortical-thickness principal component 1 and subcortical gray-matter volume principal component 1. None of these measures were associated with a subsequent change in the continuous DAT ratio (all FDR-adjusted $q \geq 0.57$; Fig. 2a). Accordingly, the primary longitudinal model provided no evidence that these broad MRI phenotypes were associated with subsequent dopaminergic changes.

We next screened seven prespecified subcortical regions. Whole-thalamus volume showed the strongest association and was the only regional measure to survive FDR correction across the seven-region family: each 1-s.d. larger baseline thalamic volume was associated with an additional 0.018-unit annual decline in the continuous DAT ratio ($\beta = -0.018$, 95% CI -0.031 to -0.005; $P = 0.007$, $q = 0.046$; Fig. 2a,b). Pallidal volume showed a weaker nominal association ($\beta = -0.012$, $P = 0.039$) that did not survive correction ($q = 0.137$), whereas the other five regions showed no evidence of association. The thalamic effect remained robust across several sensitivity analyses. Among the 334 participants with complete baseline motor data, the complete-case mixed-effects model produced a similar estimate ($\beta = -0.017$, 95% CI -0.030 to -0.004; $P = 0.009$). After further adjustment for the baseline MDS- Unified Parkinson's Disease Rating Scale Part III (UPDRS-III) score, the association remained significant in both models ($\beta = -0.019$, 95% CI -0.033 to -0.006; $P = 0.004$) and the generalized estimation equation ($\beta = -0.019$, 95% CI -0.037 to -0.001; $P = 0.037$). Under the original covariate specification, the generalized estimation equation yielded a similar negative point estimate, although the confidence interval crossed zero ($\beta = -0.018$, $P = 0.060$; Fig. 2c). Model-implied DAT changes further illustrated that a larger baseline thalamic volume corresponded to faster subsequent DAT decline (Fig. 2d).

Longitudinal associations with subsequent changes in the DAT ratio were distributed across multiple nuclei

To localize the whole-thalamus association to specific nuclei, we applied the same primary longitudinal model to 25 thalamic nuclei represented by bilateral mean volumes. Five nuclei survived FDR correction within the 25-nucleus family: the ventromedial nucleus (VM; $\beta = -0.021$, $q = 0.009$), paracentral nucleus (Pc; $\beta = -0.020$, $q = 0.021$), parafascicular nucleus (Pf; $\beta = -0.018$, $q = 0.021$), medial mediodorsal nucleus (MDm; $\beta = -0.017$, $q = 0.050$) and ventral lateral anterior nucleus (VLa; $\beta = -0.016$, $q = 0.050$) (Fig. 3a; Table 2). All five interaction estimates were negative, indicating that larger baseline nucleus volumes were associated with a faster subsequent decline in the continuous DAT ratio. These nuclei spanned the medial, intralaminar and ventral nuclear groups, indicating that the whole-thalamus association involved multiple nucleus families rather than a single anatomical subdivision (Fig. 3a,b). Covariate-adjusted association plots showed negative fitted relationships for all five nuclei, with larger baseline volumes corresponding to more negative estimated annual DAT ratio changes (Fig. 3c–g). The concordant direction across MDm, Pc, Pf, VLa and VM was consistent with the interaction estimates from the primary longitudinal models.

The thalamic pattern extended beyond conventional anatomical boundaries

Following the 25-nucleus screen showing that the association was distributed across multiple thalamic nuclei, we broadened the anatomical scope by placing all 25 nuclei and seven comparison subcortical regions (caudate, putamen, pallidum, hippocampus, amygdala, accumbens and VentralDC) in a single 32-region analysis family and reapplied FDR correction (Supplementary Table S1). Three thalamic nuclei with the strongest associations on the initial screen remained significant: VM ($\beta = -0.021$, $P < 0.001$, $FDR = 0.011$), Pc ($\beta = -0.020$, $P = 0.002$, $FDR = 0.020$) and Pf ($\beta = -0.018$, $P = 0.002$, $FDR = 0.020$) (Fig. 4a). MDm and VLa retained negative effect estimates but fell just beyond the

Table 2: **Longitudinal associations between baseline thalamic nucleus volumes and subsequent changes in the DAT ratio**

Nucleus	Anatomical family	β (year^{-1} SD^{-1})	95% CI	P value	FDR q value
AV	Anterior	−0.007	−0.019, 0.006	0.291	0.466
LD	Lateral	0.001	−0.011, 0.013	0.890	0.952
LP	Lateral	−0.002	−0.014, 0.010	0.756	0.899
MDl	Medial	−0.014	−0.026, −0.002	0.028	0.086
MDm	**Medial**	**−0.017**	**−0.029, −0.004**	**0.010**	**0.050***
MV(Re)	Medial	−0.007	−0.020, 0.006	0.298	0.466
CL	Intralaminar	0.000	−0.011, 0.011	0.952	0.952
CM	Intralaminar	−0.014	−0.026, −0.002	0.021	0.081
CeM	Intralaminar	−0.012	−0.024, 0.001	0.074	0.169
Pc	**Intralaminar**	**−0.020**	**−0.033, −0.007**	**0.003**	**0.021***
Pf	**Intralaminar**	**−0.018**	**−0.030, −0.007**	**0.002**	**0.021***
Pt	Intralaminar	−0.005	−0.018, 0.007	0.384	0.564
VA	Ventral	−0.010	−0.023, 0.002	0.101	0.194
VAmc	Ventral	−0.012	−0.025, 0.000	0.056	0.141
VLa	**Ventral**	**−0.016**	**−0.028, −0.004**	**0.010**	**0.050***
VLp	Ventral	−0.014	−0.025, −0.002	0.023	0.081
VM	**Ventral**	**−0.021**	**−0.032, −0.009**	**< 0.001**	**0.009***
VPL	Ventral	−0.012	−0.024, −0.001	0.039	0.108
LGN	Posterior	−0.010	−0.021, 0.002	0.094	0.194
MGN	Posterior	0.002	−0.010, 0.013	0.753	0.899
L-Sg	Posterior	0.003	−0.008, 0.015	0.547	0.719
PuA	Posterior	−0.008	−0.021, 0.006	0.257	0.459
PuI	Posterior	−0.004	−0.015, 0.007	0.456	0.633
PuL	Posterior	−0.001	−0.012, 0.011	0.908	0.952
PuM	Posterior	0.000	−0.011, 0.012	0.945	0.952

β denotes the time-by-baseline nucleus-volume interaction from the primary longitudinal mixed-effects model and represents the difference in annual DAT-ratio change associated with a one-standard-deviation larger baseline nucleus volume. Nucleus volumes were averaged across hemispheres, adjusted for estimated total intracranial volume and scanner-related factors, and standardized. FDR correction was applied across all 25 nucleus-level tests. Asterisks indicate $q < 0.05$ based on unrounded values. The analysis included 340 participants contributing 520 datasets.
AV, anteroventral; LD, laterodorsal; LP, lateral posterior; MDl, lateral mediodorsal; MDm, medial mediodorsal; MV(Re), reuniens (medial ventral); CL, central lateral; CM, central medial; CeM, centromedian; Pc, paracentral; Pf, parafascicular; Pt, paratenial; VA, ventral anterior; VAmc, ventral anterior magnocellular; VLa, ventral lateral anterior; VLp, ventral lateral posterior; VM, ventromedial; VPL, ventral posterolateral; LGN, lateral geniculate; MGN, medial geniculate; L-Sg, limitans–suprageniculate; PuA, anterior pulvinar; PuI, inferior pulvinar; PuL, lateral pulvinar; PuM, medial pulvinar; CI, confidence interval; DAT, dopamine transporter; FDR, false discovery rate.

significance threshold after correction across the expanded family (MDm: $\beta = -0.017$, $P = 0.010$, $FDR = 0.053$; VLa: $\beta = -0.016$, $P = 0.010$, $FDR = 0.053$). Notably, VentralDC, one of the comparison regions, also survived FDR correction ($\beta = -0.020$, $P = 0.001$, $FDR = 0.012$). Its effect ranked third in absolute magnitude among all 32 regions and was similar to those observed for VM and Pc. Thus, the expanded screen preserved a predominantly thalamic pattern while showing that the association was not strictly confined to conventional thalamic anatomical boundaries.

The identification of VentralDC raised a further question: did the longitudinal association depend on the five initially selected nuclei, or would it persist across broader anatomical definitions? To address this question, we first combined the standardized volumes of MDm, Pc, Pf, VLa and VM into an equal-weight post hoc five-nucleus composite. We then constructed an expanded nine-nucleus composite by adding MDl, CM, VA and VLp, incorporating VentralDC into a further composite, and including the whole-thalamus volume as a reference. The association did not diminish or disappear as the score definition was expanded (Fig. 4b; Supplementary Table S2). The five-nucleus composite

remained negatively associated with the change in the annual DAT ratio in both linear mixed-effects model (MixedLM, $\beta = -0.024$, $FDR = 0.001$) and generalized estimating equation (GEE $\beta = -0.023$, $FDR = 0.015$). Similar estimates were obtained for the expanded nine-nucleus composite (MixedLM: $\beta = -0.021$, $FDR = 0.001$; GEE: $\beta = -0.020$, $FDR = 0.021$). Incorporating VentralDC produced almost unchanged estimates (MixedLM: $\beta = -0.021$, $FDR = 0.001$; GEE: $\beta = -0.021$, $FDR = 0.021$). By comparison, whole-thalamus volume remained negatively associated with the change in the DAT ratio in MixedLM ($\beta = -0.018$, $FDR = 0.007$), whereas its confidence interval crossed zero in GEE ($\beta = -0.018$, $FDR = 0.060$). The three composite scores were strongly correlated with one another ($r = 0.985$–0.996). In comparison, their correlations with whole-thalamus volume were relatively lower ($r = 0.845$–0.861; Fig. 4c). Thus, the association was not restricted to the exact original five-nucleus definition and remained similar after expanding the nucleus set or incorporating VentralDC. Moreover, the high correlations among the composite scores indicated that they captured largely overlapping structural variation rather than independent signals.

The thalamic pattern showed a stable direction but variable inclusion of nucleus

Although the alternative composite definitions yielded highly consistent associations, this score-level concordance did not establish whether the five initially identified nuclei would be repeatedly selected across resampled datasets. We therefore performed 500 participant-clustered bootstrap resamples, refitting all 25 nucleus models and selecting the five nuclei with the most negative effect estimates in each resample. VM and Pc showed the highest top five selection frequencies, appearing in 83.2% and 79.8% of the resamples, respectively. Pf and MDm were selected in 65.6% and 59.6% of the resamples, respectively, whereas VLa was selected in 45.6% (Fig. 4d; Supplementary Table S3). In contrast to this variability in ranking, all five nuclei showed negative effect estimates in more than 96% of the resamples: 99.6% for both VM and Pf, 98.2% for Pc, 97.8% for MDm and 96.6% for VLa. This distinction was also evident in the overlap of the selected nucleus sets. Each resample recovered a mean of 3.34 of the original five nuclei; three and four nuclei were recovered in 41.8% and 40.8% of the resamples, respectively, whereas the exact original five-nucleus set was recovered in only 19 resamples (3.8%; Fig. 4e). Thus, resampling supported a stable negative direction and a recurrent core of thalamic nuclei, whereas variation among nuclei near the selection boundary did not support a fixed five-nucleus set.

The bootstrap analysis supported directional stability, but nucleus selection was still performed within repeated samples drawn from the same cohort; therefore, selection-related optimism could be retained. To address this issue, we conducted 20 repetitions of fully nested fivefold cross-fitting, with training and validation folds grouped by study site. Within each repetition, all participants from the same site were assigned to a single validation fold. Nucleus selection, adjustment for estimated total intracranial volume and scanner-related factors, and variable standardization were performed exclusively within the training data, with validation participants excluded from every step. The interaction estimates were negative in all 20 repetitions, ranging from $\beta = -0.019$ to -0.008, and 17 reached nominal statistical significance ($P < 0.05$; Fig. 4f). A MixedLM based on the consensus out-of-fold score also showed a significant negative association ($\beta = -0.014$, 95% confidence interval, -0.026 to -0.003; $P = 0.017$). Although this estimate was smaller in magnitude than that obtained for the post hoc five-nucleus composite in the full sample ($\beta = -0.024$), its direction remained consistent across all repetitions. Thus, the negative association between the thalamic structural score and the subsequent decrease in the DAT ratio persisted when the validation data were fully excluded from nucleus selection and preprocessing, further supporting the internal directional stability of the association.

Greater thalamic volume was associated with lower concurrent clinical burden

The preceding longitudinal analyses revealed that larger baseline thalamic structural measures were associated with faster subsequent decreases in the DAT ratio. This finding raised a distinct but complete

question: what clinical state did the same thalamic structural differences represent at the time of MRI acquisition? In the PPMI cohort, after adjustment for age, sex, baseline DAT ratio and rapid eye movement sleep behavior disorder status (RBD), each 1-SD increase in baseline whole-thalamus volume was associated with a 1.142-point decrease in the UPDRS-III score ($\beta = -1.142$; 95% confidence interval, -2.024 to -0.260; $P = 0.011$; $FDR = 0.056$; $n = 335$; Fig. 5a; Supplementary Table S4). After correction across five clinical endpoints, these results approached but did not meet the FDR significance threshold. Consistent with this pattern, the post hoc five-nucleus composite remained associated with lower UPDRS-III scores after correction across the four score definitions. Each 1-SD larger composite score was associated with a 0.790-point lower UPDRS-III score ($\beta = -0.790$, 95% confidence interval, -1.465 to -0.115; $P = 0.022$, $FDR = 0.022$; $n = 335$; Supplementary Table S5). Thus, within the same PPMI cohort, larger thalamic structural measures associated with faster subsequent DAT decline were also associated with milder motor involvement at the time of MRI. This contrast between concurrent clinical status and subsequent dopaminergic trajectory motivated us to examine whether greater thalamic volume was similarly associated with milder clinical involvement in the independent QPN-NC cohort of participants with clinically established PD. The design of the independent QPN-NC clinical-support analysis is summarized in Fig. 1d.

In the QPN-NC cohort of participants with clinically established PD, whole-thalamus volume showed a motor association in the same direction as that observed in the PPMI. Then characteristics of the endpoint-specific QPN-NC clinical-analysis samples are summarized in Table 3. After adjustment for age, sex, estimated total intracranial volume and disease duration, each 1-SD increase in thalamic volume was associated with a 4.382-point lower UPDRS-III score ($\beta = -4.382$, 95% confidence interval, -8.570 to -0.194; $P = 0.040$, $FDR = 0.040$; $n = 125$; Fig. 5b; Supplementary Table S6). This relationship was more pronounced for overall disease stage: each 1-SD increase in thalamic volume was associated with 68% lower odds of being in a higher Hoehn–Yahr stage ($OR = 0.320$, 95% confidence interval, 0.175–0.585; $P < 0.001$, $FDR < 0.001$; $n = 125$; Fig. 5c). Notably, the clinical association was not confined to motor phenotypes. Greater thalamic volume was also associated with higher Montreal Cognitive Assessment (MoCA) scores, with each 1-SD increase corresponding to a 1.709-point higher score ($\beta = 1.709$, 95% confidence interval, 0.654–2.763; $P = 0.001$, $FDR = 0.002$; $n = 110$; Fig. 5d). All three QPN-NC outcomes remained significant after FDR correction within the same analysis family. Thus, in an independent clinical PD cohort, a greater thalamic volume was consistently associated with milder motor symptoms, a lower overall disease stage and better cognitive performance, indicating the formation of a coherent cross-domain pattern of concurrent clinical involvement.

Discussion

By integrating baseline MRI with longitudinal DAT and clinical phenotyping, we identified a relationship between thalamic structure and distinct temporal dimensions of PD. Unlike broad MRI summary measures, larger baseline whole-thalamus volume was associated with faster subsequent decreases in the DAT ratio, with negative estimates broadly maintained across alternative model specifications and resampling analyses. Anatomical localization further revealed that this association spanned nuclei from the medial, intralaminar and ventral groups, whereas expanded regional screening revealed a comparable effect in the ventral diencephalic region, suggesting a thalamus-centred structural pattern extending into adjacent diencephalic territory. Notably, greater thalamic volume was associated with less concurrent clinical burden in both the PPMI cohort and the independent QPN-NC cohort but with faster subsequent decrease in the DAT ratio in the PPMI cohort. Together, these findings position thalamic morphology at the interface between current clinical expression and subsequent dopaminergic changes, providing a systems-level structural perspective on why clinical state and molecular-imaging progression may not evolve in parallel in PD.

The emergence of a thalamic signal against a background of null associations for broad MRI

Table 3: Characteristics of participants with Parkinson's disease included in the QPN-NC clinical analyses

Characteristic	UPDRS-III and Hoehn–Yahr analyses	MoCA analysis
Participants included	125	110
Demographic and imaging characteristics		
Age at MRI, years	66.07 (9.69)	65.87 (9.25)
Sex, male/female	88/37 (70.4%/29.6%)	74/36 (67.3%/32.7%)
Disease duration, years	3.64 [1.54–7.04]	3.67 [1.43–6.86]
Estimated total intracranial volume, mm^3	1,592,677 (171,110)	1,595,694 (180,953)
Whole-thalamus volume, mm^3	13,897 (1,559)	13,912 (1,639)
Clinical characteristics		
UPDRS-III score	30 [22–40]	–
Observed range	5–86.7	–
Hoehn–Yahr stage	2 [2–3]	–
Observed range	1–4	–
MoCA total score	–	25 [23–28]
Observed range	–	15–30

Data are presented as mean (s.d.), median [interquartile range], range, or n (%), as appropriate. QPN-NC release 1 comprised 271 participants, including 202 participants with clinically diagnosed Parkinson's disease and 69 controls. The primary clinical analyses were restricted to participants with Parkinson's disease and complete data for the corresponding outcome, whole-thalamus volume, estimated total intracranial volume, age, sex and disease duration. UPDRS-III and Hoehn–Yahr analyses included the same 125 participants; the MoCA analysis included 110 participants. MoCA, Montreal Cognitive Assessment; QPN-NC, Quebec Parkinson Network Neuroimaging Cohort; UPDRS-III, Unified Parkinson's Disease Rating Scale Part III.

phenotypes may reflect the hub position of the thalamus within dopamine-sensitive networks. The basal ganglia communicate with motor, associative and limbic cortical territories through multiple functionally segregated but coordinated loops passing through the thalamus, placing it at a key junction through which basal ganglia output influences cortical information processing[9]. Nigrostriatal dopamine depletion in PD not only alters striatal and basal ganglia output but is also accompanied by widespread reorganization of neuronal firing patterns, oscillatory activity and synchronization across the basal ganglia-thalamocortical network[27]. Thalamostriatal projections, to which the intralaminar nuclei make a major contribution, provide glutamatergic regulation of striatal neurons and undergo structural and functional alterations in parkinsonian states[10]. Human imaging studies similarly identify microstructural abnormalities in selected thalamic projection fibers in patients with untreated early PD, together with altered functional connectivity of thalamic subdivisions[17;18]. Within this network context, whole-thalamus volume may integrate structural differences distributed across multiple motor and associative circuits, potentially explaining why the thalamic association was detectable when broad cortical and subcortical structural measures showed no corresponding effects.

Anatomical localization at the nucleus level further indicated that the whole-thalamus association was not driven by a single relay nucleus but was distributed across ventral, intralaminar and medial thalamic systems with complementary connectivity profiles. Basal ganglia-thalamocortical pathways are themselves organized into multiple parallel but interacting motor, associative and limbic circuits, allowing distinct thalamic nuclei to integrate different functional pathways into a systems-level disease phenotype[9;16]. VLa and VM lie within motor thalamic pathways and participate in transmitting basal ganglia-related outputs to motor and premotor cortices, whereas previous studies have reported

structural and functional differences in the motor thalamus across PD motor subtypes[28;29]. Pc and Pf belong to the intralaminar system, which is extensively connected with the striatum and cortical regions and contributes to action selection, attention and behavioural-state regulation; MDm extends this structural pattern into the medial thalamic territory associated with prefrontal and higher-order adaptive processing[10]. The joint involvement of these nuclei therefore provides an anatomical link across motor output, thalamostriatal regulation and cognitive control. Consistent with this interpretation, imaging studies in patients with untreated PD have revealed differences in thalamic nucleus volume and intrinsic thalamic structural organization among motor subtypes, whereas more recent work has related specific changes in the volume of the nucleus to both motor and cognitive manifestations[19;23]. In the present study, all five FDR-significant nuclei showed negative effects, and the expanded nine-nucleus composite retained a similar association magnitude, further suggesting that the whole-thalamus result reflects a distributed structural pattern jointly formed by several related nuclei rather than an isolated contribution from any single nucleus.

The joint 32-region screen further extended the anatomical boundary of this distributed pattern. Although the strongest FDR-corrected associations remained concentrated in VM, Pc and Pf, the effects of VentralDC also survived correction and were comparable to those of the leading thalamic nuclei. In the FreeSurfer segmentation framework, VentralDC does not represent a single histologically homogeneous nucleus but is a composite region defined using conventional MRI boundaries that encompass through several ventral diencephalic structures and part of the ventral tegmentum[30;31]. These structures are spatially adjacent to the thalamus, subthalamus and midbrain and collectively participate in basal ganglia-related motor, arousal and limbic networks, which is consistent with the broader view of PD as a systems-level disorder affecting multiple interconnected circuits[16]. Previous MRI studies have also revealed volumetric alterations in the subthalamic and adjacent red nucleus regions in patients with PD, further indicating that disease-related morphological differences may involve structures surrounding the thalamus across the diencephalic and midbrain territories[32]. The findings of the ventralDC finding may therefore reflect an extension of the thalamus-related structural signal across conventional atlas boundaries rather than an independent signal competing with the thalamic association. The nearly identical effects of the expanded nine-nucleus composite before and after the addition of VentralDC further indicate that VentralDC complemented, but did not displace, the thalamic nuclear core of this anatomical pattern.

The independent QPN-NC cohort further revealed that the association between greater thalamic volume and milder clinical involvement was consistent across cohorts and clinical domains. UPDRS-III, Hoehn–Yahr stage and MoCA score capture motor impairment, overall disease stage and cognitive status, respectively. Their concordant directions indicate that the clinical relevance of the thalamic structure is not restricted to a single symptom or assessment scale. Previous studies have similarly linked thalamic volume, functional connectivity and intrinsic structural organization to motor subtypes and motor severity in PD[14;19;28;29]. Nucleus-level volumes and lateralization patterns have also been associated with both motor measures and cognitive performance[23]. The QPN-NC findings therefore extend the clinical relevance of thalamic structure to an independent sample and across motor, disease-stage and cognitive outcomes.

Considering the longitudinal DAT findings, these clinical associations raise the possibility that the thalamus contributes to buffering the clinical expression of dopaminergic loss. Motor symptoms of PD typically fully manifest only after substantial nigrostriatal dopaminergic loss. This clinical–pathological discrepancy has long been attributed to compensatory mechanisms both within and beyond the dopaminergic system[33]. Particularly relevant to the present findings, greater thalamic microstructural integrity has been associated with greater motor reserve in patients with untreated early PD. Functional imaging studies have also revealed increased connectivity of thalamic subdivisions and enhanced recruitment of cerebello-thalamo-cortical circuits[18;34–36]. DAT decline primarily reflects changes in nigrostriatal dopaminergic terminals, whereas motor and cognitive performance emerge from

the combined activity of several distributed brain networks. These include basal ganglia–thalamocortical, cerebello-thalamo-cortical and association-cortical systems. Greater thalamic structure may therefore help maintain the integration of these networks, allowing relatively mild clinical manifestations to coexist temporarily with continuing or faster DAT decline. A complementary possibility is that this asynchrony is stage dependent. Individuals with greater structural reserve may remain mildly affected while the nigrostriatal system has already entered a period of more rapid change. As network-level buffering diminishes, clinical progression may subsequently track dopaminergic changes more closely[37;38]. Within this framework, the observed combination is not directionally contradictory but may reflect thalamic network buffering and nigrostriatal changes operating over different timescales.

This study has several limitations. First, thalamic structural measures were derived from a single baseline MRI assessment and therefore cannot distinguish whether a larger thalamus represents premorbid structural reserve or an adaptive feature that emerges or is preserved during the disease course. Second, the longitudinal association between thalamic volume and subsequent DAT decline was identified in a single cohort, whereas QPN-NC provided independent support based on concurrent motor severity, disease stage and cognitive status. This relationship between structural variation and molecular-imaging trajectories therefore requires further evaluation in independent samples with longitudinal MRI, DAT imaging and clinical follow-up. Third, relatively small thalamic nuclei, including VM, Pc and Pf, as well as the anatomically heterogeneous VentralDC, were defined using automated segmentation and predefined atlas boundaries. Some associations may consequently be influenced by segmentation precision and anatomical definitions. Higher-resolution structural imaging, individualized nucleus segmentation, and diffusion or functional-connectivity measures could help determine whether the associations across these regions reflect a common thalamo-basal ganglia network.

In summary, this study revealed a longitudinal association between thalamic structure and subsequent decreases in DAT among multilevel baseline MRI phenotypes, localized this signal to multiple thalamic nuclei, and revealed an association of similar magnitude in the ventral diencephalic region. Greater baseline thalamic volume was associated with faster subsequent DAT decline but less severe concurrent motor and cognitive involvement. By linking greater thalamic volume to both less severe concurrent clinical involvement and faster subsequent DAT decline, these findings indicate that brain structure, current clinical state and subsequent molecular-imaging changes are not related through a simple one-to-one correspondence. This study thereby connects whole-thalamus volume, nucleus-level localization, longitudinal DAT changes and clinical phenotypes across cohorts, providing convergent multimodal imaging and clinical evidence for understanding the temporal relationships among brain structure, dopaminergic progression and clinical involvement in PD.

Methods

Study design and participants

This study used two cohorts. The primary longitudinal analysis was based on data from the PPMI, an international multicentre observational study designed to investigate biomarkers of PD through standardized clinical assessments, biospecimen collection and multimodal imaging[24]. Data were obtained from the PPMI database on 5 March 2026 following approval of the data-access request. Participants were required to be positive for cerebrospinal fluid α-synuclein seed amplification activity[7]; to have no clinical diagnosis of PD at baseline; and to have a negative baseline DAT-SPECT scan, defined as a lowest-putamen observed-to-expected ratio of at least 0.65, with expected values determined by age and sex. Participants were additionally required to have an available T1-weighted MRI acquired within 180 days of the baseline DAT-SPECT scan, successful linkage of imaging and clinical data, and at least one calculable DAT-SPECT scans obtained after both the baseline DAT-SPECT scan and the selected MRI. The initial cohort comprised 361 participants who were α-synuclein SAA positive, DAT

negative and without a clinical diagnosis of PD at baseline. Baseline structural MRI data from 341 participants passed morphometric processing and quality control. One additional participant lacked calculable post-MRI DAT data. A final longitudinal sample of 340 participants from 33 study sites, contributing 520 post-MRI DAT datasets were included.

The QPN-NC was used to independently validate the association between thalamic structure and contemporaneous clinical status observed in PPMI. QPN-NC release 1 comprised 271 participants, including 202 individuals with clinically diagnosed PD and 69 control participants[25;26]. The primary clinical analyses were restricted to participants with PD whose bilateral thalamic volumes, estimated total intracranial volume, age, sex, disease duration and corresponding clinical outcomes were available. On the basis of endpoint-specific data completeness, 125 participants were included in the UPDRS-III and Hoehn–Yahr stage analyses, and 110 participants were included in the Montreal Cognitive Assessment analysis. Control participants were not included in these primary models of clinical disease severity.

The original PPMI study protocols were approved by the institutional review board or independent ethics committee at each participating site, and all participants provided written informed consent in accordance with the Declaration of Helsinki. The principal PPMI protocols included Protocol 001, approved by the University of Rochester Research Subjects Review Board (RSRB no. 00031629), and Protocol 002, approved by the WCG Institutional Review Board (tracking no. 20200597). QPN-NC data collection was approved by the McGill University Health Centre Research Ethics Board under the QPN protocols 2015-143, MP-CUSM-NEU-14-053 and MP-37-2015-143, and all participants provided written informed consent. The present study used only anonymous de-identified data obtained through approved access procedures and complied with the corresponding data-use agreements.

DAT imaging and longitudinal assessment

DAT-SPECT imaging was performed according to standardized PPMI procedures using [^{123}I]ioflupane (DaTscan)[39]. Participants received thyroid blockade before slow intravenous administration of 111–185 MBq (3–5 mCi) of the radiotracer, followed by 15–20 ml of normal saline. Imaging commenced 4 h ($\pm$30 min) after injection. Projection data were acquired using low-energy high-resolution parallel-hole collimators, a 128×128 matrix, 60 projections per detector at 3° increments and 30 s per projection, with a 20% energy window centred at 159 keV.

PPMI provided quantitative DAT-SPECT measurements processed centrally by its imaging core laboratory[24]. Raw projection data were reconstructed in HERMES using the HOSEM algorithm. The reconstructed images underwent zero-order Chang attenuation correction and Gaussian smoothing with a 6-mm full width at half maximum. Quantitative analysis was performed in MIAKAT (version 5.0), including affine registration to MNI152 space and application of the CIC atlas. Regional SBRs were calculated as $(\mathrm{SUV}_{\mathrm{target}}/\mathrm{SUV}_{\mathrm{reference}}) - 1$, using cerebral white matter as the reference region[39].

For each DAT-SPECT scan, we extracted the left and right whole-putamen SBRs referenced to cerebral white matter and retained the lower value to represent the more affected side. The expected putamen SBR was calculated using the prespecified age- and sex-standardization procedure adopted in the PPMI curated data. The continuous DAT ratio was defined as follows:

$$\text{DAT ratio} = \frac{\min\left(\text{left putamen SBR, right putamen SBR}\right)}{\text{expected putamen SBR}}.$$

A higher DAT ratio indicated greater putamen DAT binding than expected for the participant's age and sex. A baseline DAT ratio of at least 0.65 was used only to define DAT-negative status at cohort entry. In the longitudinal analyses, all follow-up DAT ratios were retained as continuous measures to preserve gradual variation above and below this threshold.

Longitudinal time was anchored to the baseline DAT-SPECT scan. Intervals between DAT assessments were calculated as the difference between scan dates divided by 365.25 and expressed in years.

The primary analysis included only DAT-SPECT scans acquired after both the baseline DAT-SPECT scan and the selected baseline MRI. The baseline DAT ratio was included as a covariate and was not treated as a post-MRI repeated outcome.

The primary longitudinal outcome comprised the continuous DAT ratios from all post-MRI follow-up assessments. Annual changes in the DAT ratio and their associations with each baseline MRI measurement were estimated directly from the repeated-measures model. Specifically, the main effect of time represented the longitudinal change, whereas the interaction between time and the baseline MRI measurement represented its imaging-related difference. This approach avoided calculating a separate annual slope for each participant. The interaction coefficient represented the additional annual change in the DAT ratio associated with a 1-SD larger baseline MRI measure.

Baseline MRI acquisition and preprocessing

Baseline MR images in the PPMI included T1-weighted structural and neuromelanin-sensitive images acquired on the same day and scanner. The primary analysis required MRI acquisition within 180 days of both baseline cerebrospinal fluid α-synuclein SAA and baseline DAT imaging. Structural T1-weighted MRI was acquired at 3 T using Siemens ($n = 284$) or GE ($n = 56$) scanners. Acquisition sequences included 3D MPRAGE ($n = 270$), spoiled gradient echo ($n = 56$) and gradient echo ($n = 14$). Images were reconstructed using a 256×256 matrix with a slice thickness of 1.0–1.2 mm; 336 of 340 scans had 1.0-mm isotropic voxels. Across the approved site- and scanner-specific protocols, repetition time (TR) ranged from 6.608 to 2300 ms, echo time (TE) from 1.92 to 3.22 ms and flip angle from 9° to 11°, whereas inversion time was protocol dependent. Neuromelanin-sensitive MRI was acquired using a 2D gradient-echo sequence with magnetization-transfer preparation, with an in-plane resolution of 0.491–0.545 mm and a slice thickness of 1.5–2.0 mm. The standard $0.5 \times 0.5 \times 1.5$-mm acquisition was used in 259 of 340 participants. The nominal TR was approximately 465 ms, observed TE ranged from 2.88 to 5.00 ms, the flip angle ranged from 32° to 40°, and five repeated measurements were nominally acquired. Because PPMI imaging was obtained across 33 study sites, these values reflect the observed acquisition parameters of the analytic sample under the approved site- and scanner-specific protocols. Nominal neuromelanin-sensitive MRI TR and repeat number were taken from the acquisition protocol because the exported repetition-time fields were not directly comparable across scanner platforms. Scanner and acquisition parameters were retained for subsequent adjustment.

T1-weighted images were processed using the standard `recon-all` pipeline in FreeSurfer 7.4.1 to obtain cortical reconstructions and subcortical segmentations[30;31]. Cortical thickness, subcortical gray-matter volume and estimated total intracranial volume were subsequently extracted. Repeated neuromelanin-sensitive image frames were rigidly registered, intensity-normalized and averaged before alignment to the corresponding T1-weighted image. After bias-field correction, the T1-weighted image was registered to MNI standard space, and a midbrain atlas containing the bilateral substantia nigra/ventral tegmental area and cerebral peduncle reference regions was transformed into individual space.

Quality control assessed target-region coverage, repeat-frame registration, cross-modal alignment and atlas localization. Among the 361 participants, neuromelanin-sensitive measures were successfully derived for 347; four were excluded from the primary analysis because of insufficient reference-region coverage. Six participants with signal-intensity or asymmetry outliers but satisfactory registration were retained in the primary analysis and excluded only from a strict quality-control sensitivity analysis. After application of the 180-day imaging window and completion of morphometric quality control, 341 participants comprised the common baseline MRI analysis set.

Construction and standardization of baseline MRI measures

We first constructed four summary MRI measures representing distinct levels of brain structure. The substantia nigra/ventral tegmental area (SN/VTA) signal was defined as the mean contrast of the target region relative to the cerebral peduncle reference region. SN/VTA asymmetry was defined as the absolute difference in bilateral signals relative to the sum of the left and right signals. Both measures were adjusted for scanner category and neuromelanin-sensitive acquisition parameters and subsequently standardized. The cortical-thickness summary measure was derived from 68 bilateral FreeSurfer cortical regions, whereas the subcortical gray matter summary measure was derived from 14 bilateral volumes comprising the caudate, putamen, pallidum, thalamus, hippocampus, amygdala and nucleus accumbens. Principal component analysis was performed after adjustment of the regional measures for scanner effects; subcortical volumes were additionally adjusted for estimated total intracranial volume. The first principal component was retained as the corresponding whole-brain summary measure.

The initial regional screen included bilateral mean volumes of the caudate, putamen, pallidum and thalamus, together with bilateral mean cortical thickness of the precentral, paracentral and postcentral regions. Subcortical volumes were adjusted for estimated total intracranial volume and scanner category, whereas cortical-thickness measures were adjusted for scanner category. All MRI data were converted to standardized scores with a mean of zero and a standard deviation of one. Model coefficients therefore represent the difference in annual DAT-ratio change associated with a 1-standard-deviation larger baseline MRI measure.

Thalamic nuclei and anatomical boundary analyses

The thalamus in each hemisphere was segmented into 25 nuclei using FreeSurfer v7.4.1 and its probabilistic thalamic atlas was derived from ex vivo MRI and histology[20;21]. Quality control required all nucleus volumes to be positive and the relative difference between their summed volume and the corresponding whole-thalamus volume to be no greater than 0.1%. For each nucleus, the left and right volumes were averaged, adjusted for estimated total intracranial volume and scanner category, and standardized. The same longitudinal model was fitted separately for each of the 25 nuclei, with FDR correction applied across this 25-stage test family.

To assess whether the association was restricted to the thalamus, we subsequently combined the 25 thalamic nuclei with seven comparison regions comprising the caudate, putamen, pallidum, hippocampus, amygdala, nucleus accumbens and VentralDC in a joint 32-region screen. FDR correction was recalculated across all 32 tests. The seven comparison regions were likewise represented by bilateral mean volumes, adjusted for estimated total intracranial volume and scanner category, and standardized.

To evaluate the robustness of the findings to the precise anatomical definition, we constructed four structural measures: a post hoc five-nucleus composite comprising MDm, Pc, Pf, VLa and VM; an expanded nine-nucleus composite that additionally included MDl, CM, VA and VLp; a further composite combining the expanded nine-nucleus set with VentralDC; and whole-thalamus volume. Each composite was calculated as the equal-weight mean of its constituent standardized regional volumes and was subsequently restandardized. The four measures were analyzed using both linear mixed-effects models and generalized estimating equations, with FDR correction applied across the four tests within each model type.

Statistical analysis of longitudinal DAT change

The primary analysis used a random-intercept linear mixed-effects model with the continuous DAT ratio from each post-MRI follow-up examination as the outcome. Fixed effects included follow-up time, standardized baseline MRI measurements, their interaction, baseline DAT ratio, age, sex and rapid eye movement sleep behavior disorder status, together with the interaction of each covariate with time.

Participant-specific random intercepts accounted for within-participant repeated scans. Models were estimated by maximum likelihood. The primary parameter was the interaction between time and the baseline MRI measurement, with its coefficient representing the additional annual change in the DAT ratio associated with a 1-standard-deviation larger baseline MRI measurement.

Generalized estimating equations with a Gaussian distribution and exchangeable working correlation structure were used as a sensitivity analysis of population-averaged effects. For whole-thalamus volume, the mixed-effects model was repeated among participants with complete baseline MDS-UPDRS-III data. Baseline MDS-UPDRS-III scores and their interactions with time were then additionally included in both the mixed-effects and generalized estimating equation models. Multiple comparisons were controlled using the Benjamini–Hochberg procedure separately within the analysis families comprising the four broad MRI measures, seven initial regional measures, 25 thalamic nuclei, the joint 32-region screen and four composite measures. All tests were two-sided, with $FDR < 0.05$ considered to indicate statistical significance after multiple-comparison correction.

Resampling and cross-fitting stability of nucleus selection

We assessed the stability of the 25-nucleus screen using 500 participant-clustered bootstrap resamples. Each resample retained all longitudinal DAT-SPECT scan from the sampled participants. The 25 nucleus models were refitted, and we recorded the frequency with which each nucleus showed a negative effect, which ranked among the five most negative effects and survived FDR correction. We also quantified the overlap between each resampled five-nucleus set and the original five-nucleus set.

We additionally performed 20 repetitions of fivefold cross-fitting, with the data being partitioned by study site. Scanner and estimated total intracranial volume adjustment, standardization and five-nucleus selection were performed independently within each training set. The resulting transformations and selected nuclei were then applied to the corresponding validation set to construct an equal-weight out-of-fold composite score. The primary longitudinal mixed-effects model was fitted using the out-of-fold scores from each repetition. Finally, the 20 out-of-fold scores for each participant were averaged and restandardized to derive a consensus cross-fit score.

QPN-NC structural MRI and clinical measures

The QPN-NC analysis used T1-weighted MR derivatives from the first imaging visit. Structural images were processed using FreeSurfer 7.4.1[20;21]. Left and right thalamic volumes were obtained from the automated subcortical segmentation, and their sum was defined as the whole-thalamus volume. The estimated total intracranial volume was obtained from the same processing workflow. Whole-thalamus volume, age at MRI, estimated total intracranial volume and disease duration were standardized within the QPN-NC sample. Disease duration was defined as age at MRI minus age at clinical diagnosis.

Concurrent clinical outcomes included the harmonized UPDRS-III motor score, derived Hoehn–Yahr stage and total MoCA score. These measures were obtained from the harmonized QPN-NC clinical tables and linked to the first-visit MRI at the participant level. The median interval between MRI and the corresponding clinical assessment was 0 months. UPDRS-III and Hoehn–Yahr stages represented motor severity and overall disease stage, respectively, whereas the MoCA assessed global cognitive performance. Each analysis included participants with complete data for the corresponding outcome and model covariates.

Concurrent clinical association analyses

In the PPMI, we selected the UPDRS-III assessment closest to the MRI within a 180-day window, prioritizing examinations performed in the off-medication or untreated state when multiple records were available. Associations of whole-thalamus volume and the four structural scores with UPDRS-III scores

were examined using linear regression with HC3 heteroscedasticity-robust standard errors, adjusting for age, sex, baseline DAT ratio and rapid eye movement sleep behavior disorder status. FDR correction was applied across five clinical endpoints for the whole-thalamus analysis and across four score definitions for the structural score analysis.

In participants with PD from QPN-NC, the UPDRS-III score and MoCA score were analyzed using linear regression with robust standard errors for HC3, whereas the Hoehn–Yahr stage was analyzed using proportional odds ordinal logistic regression. All the models were adjusted for age, sex, estimated total intracranial volume and disease duration. FDR correction was applied across the three clinical outcomes, and each model used participants with complete outcome and covariate data.

Statistical software and missing data

Statistical analyses were conducted in Python using NumPy, pandas, SciPy, statsmodels and scikit-learn. Unless otherwise specified, all tests were two-sided, and the false discovery rate was controlled using the Benjamini–Hochberg procedure, with an $FDR < 0.05$ considered to indicate statistical significance after correction. Missing data were handled using model-specific complete-case analysis without imputation. Fixed random seeds were used for the resampling and cross-fitting analyses to ensure reproducibility.

Data availability

PPMI data are available to qualified researchers through the PPMI database, subject to the corresponding data-use agreement. The QPN-NC release 1 dataset is registered on Zenodo (https://doi.org/10.5281/zenodo.17246063), with access subject to approval by the data custodians. Owing to third-party data-use restrictions, participant-level data cannot be redistributed by the authors. Shareable summary results and figure source data will be made available by the authors upon reasonable request.

Acknowledgements

We thank all participants and their families in the Parkinson's Progression Markers Initiative (PPMI) and the Quebec Parkinson Network (QPN), as well as the investigators and staff involved in data collection, curation and sharing.

Data used in the preparation of this article were obtained on 5 March 2026 from the Parkinson's Progression Markers Initiative (PPMI) database (https://www.ppmi-info.org/access-data-specimens/download-data), RRID: SCR_006431. For up-to-date information on the study, please visit https://www.ppmi-info.org.

PPMI, a public–private partnership, is funded by The Michael J. Fox Foundation for Parkinson's Research and its funding partners, including AbbVie, Alamar Biosciences, Aligning Science Across Parkinson's, Arrowhead Pharma, AskBio, BIAL, BioArctic, Biohaven, BlueRock Therapeutics, Bristol-Myers Squibb, Calico Labs, Capsida Biotherapeutics, Critical Path Institute, DaCapo Brainscience, Denali, Edmond J. Safra Foundation, Eli Lilly, Gain Therapeutics, GE HealthCare, Genentech, GSK, Insitro, Johnson & Johnson Innovative Medicine, Lundbeck, Merck, Neumora, Neuron23, Novartis, Regeneron, Roche, Sanofi, Tenvie, UCB, Vanqua Bio, Voyager Therapeutics and the Weston Family Foundation.

We also acknowledge the Quebec Parkinson Network (QPN) for data collection and sharing. QPN is supported by the Fonds de recherche du Québec–Santé (FRQS).

Author contributions

Z.W., R.N. and J.H.W. conceived and designed the study. Z.W. and L.X. analysed the data. Z.W., L.X., C.W., R.N. and J.H.W. interpreted the results. J.J.W. provided clinical interpretation of the findings. C.W. contributed to methodological discussions. Z.W. prepared the figures and tables and wrote the main manuscript text. Z.W. and L.X. revised the manuscript. J.J.W., R.N. and J.H.W. critically revised the manuscript. R.N. and J.H.W. supervised the study. All authors reviewed and approved the final manuscript.

Competing interests

The authors declare no competing interests.

Funding Declaration

This research received no specific grant from any funding agency in the public, commercial, or not-for-profit sectors.

Supplementary information

Supplementary information is available in the online version of this article.

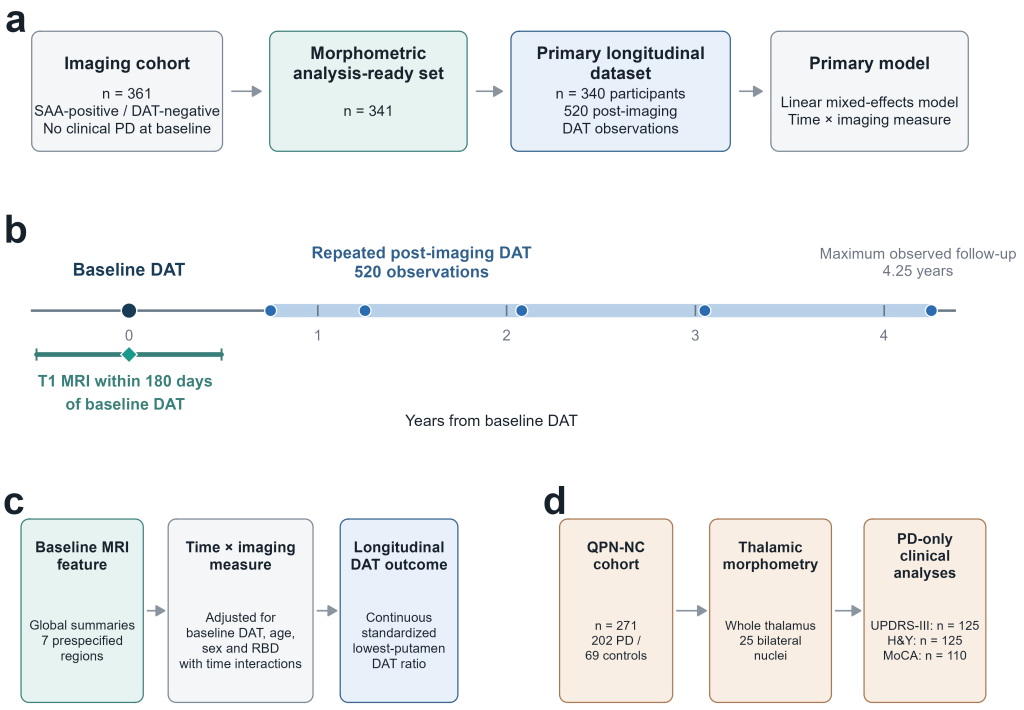

Figure 1: **Study design and analytical framework. a**, The initial PPMI imaging cohort comprised 361 SAA-positive, DAT-negative participants. Baseline morphometric quality control yielded 341 participants, of whom 340 contributed 520 calculable post-MRI DAT observations to the primary longitudinal analysis. **b**, Baseline DAT imaging defined time zero. T1-weighted MRI was acquired within 180 days before or after baseline DAT imaging, with a median absolute interval of 91 days. The median maximum follow-up per participant was 2.08 years, and the longest observed follow-up was 4.25 years. **c**, The primary estimand was the interaction between time and each baseline thalamic measure in a random-intercept linear mixed-effects model of the continuous standardized lowest-putamen DAT ratio. Models included baseline DAT, age, sex and RBD, together with the interaction of each covariate with time. **d**, The QPN-NC clinical-support cohort comprised 202 participants with clinically diagnosed PD and 69 controls. Whole-thalamus measures were evaluated in relation to MDS-UPDRS-III, Hoehn–Yahr stage and MoCA. DAT, dopamine transporter; MDS-UPDRS-III, Movement Disorder Society Unified Parkinson's Disease Rating Scale Part III; MoCA, Montreal Cognitive Assessment; MRI, magnetic resonance imaging; PD, Parkinson's disease; PPMI, Parkinson's Progression Markers Initiative; RBD, rapid eye movement sleep behavior disorder; SAA, α-synuclein seed amplification assay.

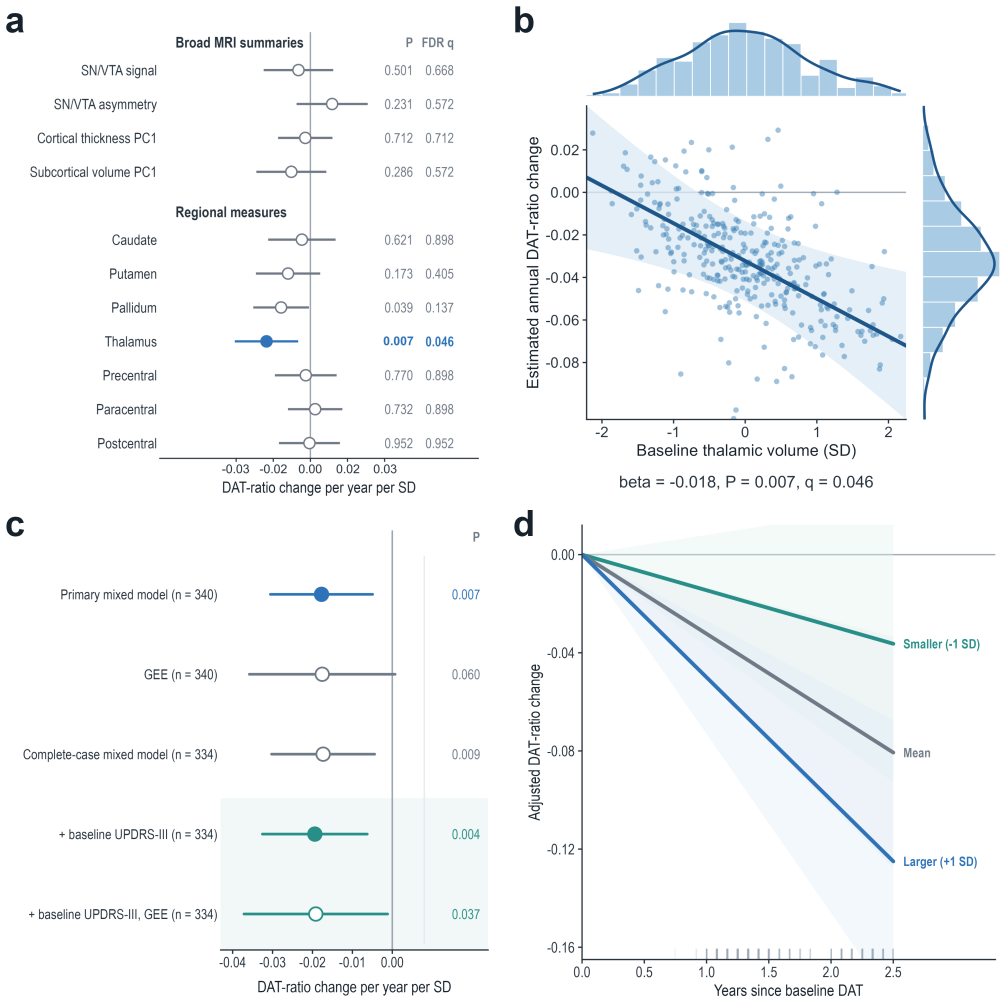

Figure 2: **Broad structural screening identified the thalamus as a correlate of subsequent DAT decline. a**, Time-by-imaging interaction estimates and 95% confidence intervals for four broad MRI summaries and seven prespecified regional measures. Nominal P values and FDR-adjusted q values are shown. Benjamini–Hochberg correction was applied separately within the four-measure broad-summary family and the seven-measure regional family. **b**, Model-adjusted joint plot of standardized baseline whole-thalamus volume and estimated annual DAT-ratio change. Points show participant-level adjusted partial residuals, the solid line shows the fitted association, shading indicates the 95% confidence interval, and marginal distributions are shown along both axes. **c**, Whole-thalamus interaction estimates from the primary mixed-effects model, population-averaged GEE, complete-case mixed-effects model, and mixed-effects and GEE models further adjusted for baseline MDS-UPDRS-III. Error bars indicate 95% confidence intervals. **d**, Model-implied adjusted DAT-ratio change at baseline whole-thalamus volumes of -1 s.d., the mean and $+1$ s.d. Shaded bands indicate 95% confidence intervals, and rug marks show the distribution of observed follow-up times. CI, confidence interval; DAT, dopamine transporter; FDR, false discovery rate; GEE, generalized estimating equation; MDS-UPDRS-III, Movement Disorder Society Unified Parkinson's Disease Rating Scale Part III; MRI, magnetic resonance imaging; SN/VTA, substantia nigra/ventral tegmental area.

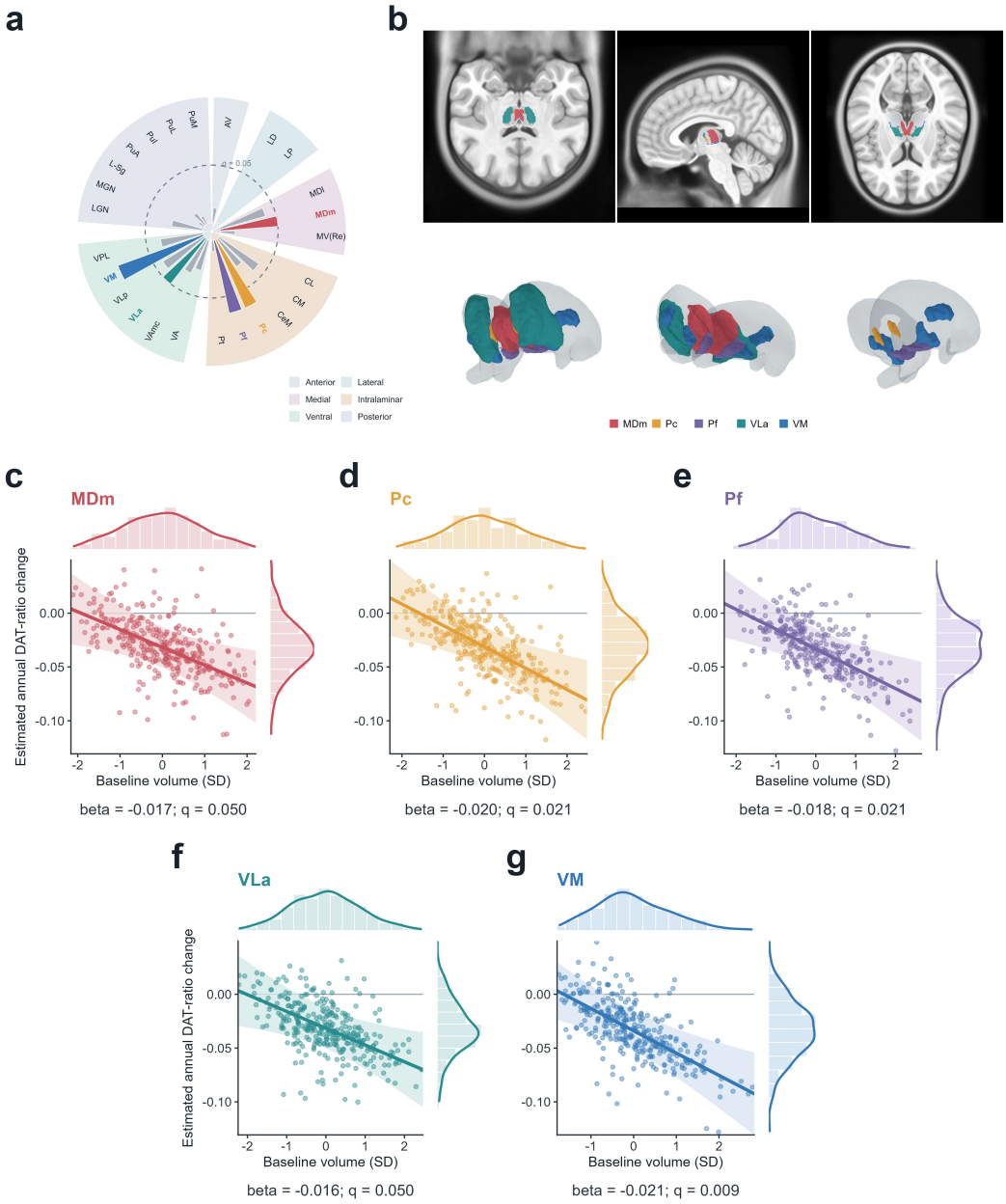

Figure 3: **The thalamic association with subsequent DAT decline was distributed across multiple nuclei. a,** Primary longitudinal mixed-effects associations for 25 bilateral mean thalamic nucleus volumes grouped into six anatomical families. Radial bars show FDR-adjusted evidence, the dashed circle denotes $q = 0.05$, and the five nuclei surviving correction are highlighted. **b,** Standard-template sections and three-dimensional views showing the locations of the five nuclei. **c–g,** Covariate-adjusted associations of baseline MDm, Pc, Pf, VLa and VM volumes, respectively, with annual DAT-ratio change. Lines and shading show fitted associations and 95% confidence intervals; marginal distributions show the data distributions. Each panel reports the longitudinal interaction estimate β and FDR-adjusted q value. Volumes were adjusted for estimated total intracranial volume and scanner-related factors and standardized. The analysis included 340 participants and 520 datasets. MDm, medial mediodorsal nucleus; Pc, paracentral nucleus; Pf, parafascicular nucleus; VLa, ventral lateral anterior nucleus; VM, ventromedial nucleus; DAT, dopamine transporter; FDR, false discovery rate.

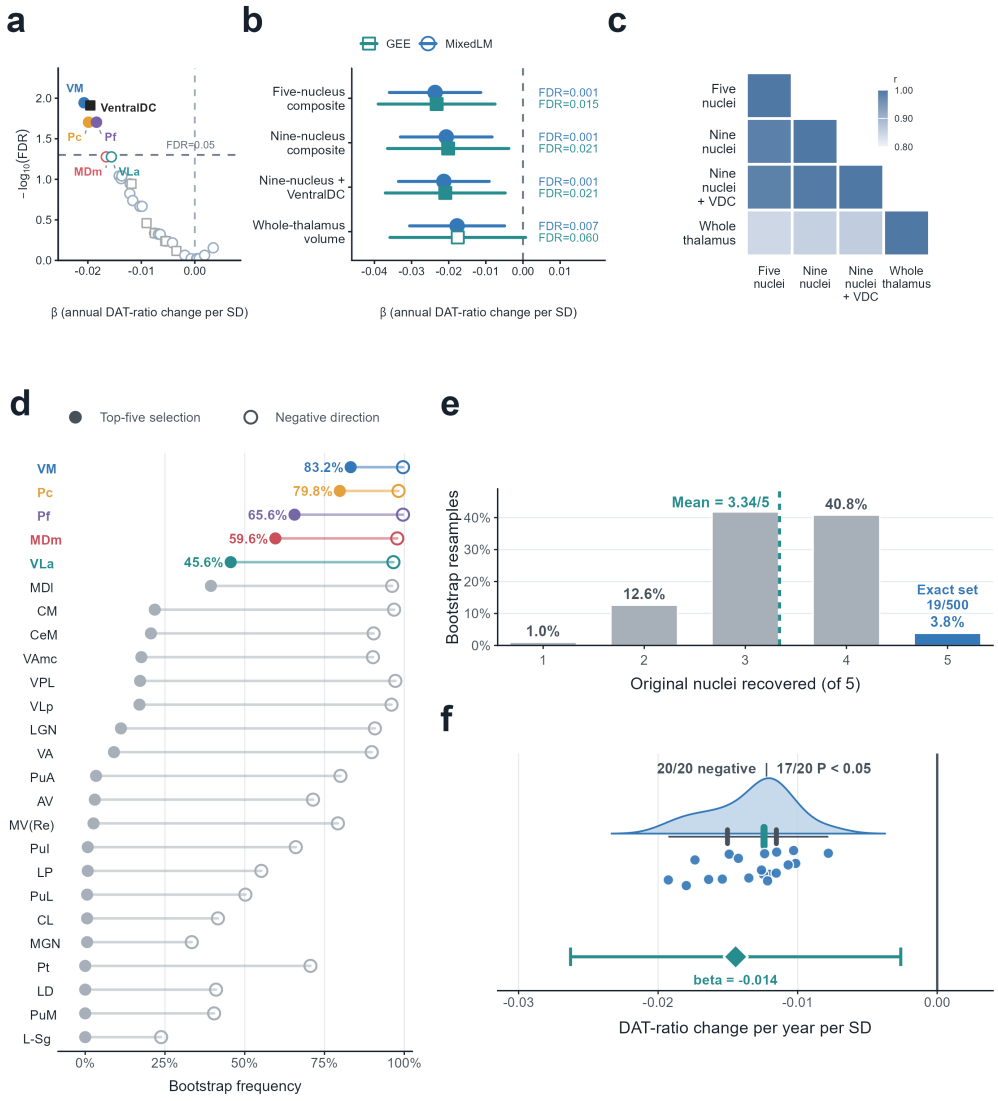

Figure 4: **Robustness and stability of the thalamic structural association. a,** Joint screening of 25 thalamic nuclei and seven comparison regions. Circles and squares indicate thalamic nuclei and comparison regions, respectively; filled symbols indicate $FDR < 0.05$. Dashed lines denote $FDR = 0.05$ and a null effect. **b,** MixedLM and GEE estimates for the five-nucleus, expanded nine-nucleus, nine-nucleus plus VentralDC and whole-thalamus scores. Horizontal lines represent 95% confidence intervals; FDR correction was applied across the four scores within each model. **c,** Pearson correlations among the four scores (off-diagonal $r = 0.845$–0.996). **d,** Top-five selection and negative-direction frequencies for 25 nuclei across 500 bootstrap resamples. **e,** Number of original nuclei recovered in each bootstrap-selected set. A mean of 3.34 of five nuclei was recovered, whereas the exact set was recovered in 19 of 500 resamples (3.8%). **f,** Effect estimates from 20 repeated site-grouped nested cross-fitting analyses. All estimates were negative and 17 had $P < 0.05$. The consensus out-of-fold estimate was $\beta = -0.014$ (95% confidence interval, -0.026 to -0.003; $P = 0.017$). Scores were equal-weight averages of standardized volumes adjusted for estimated total intracranial volume and scanner-related factors. Analyses included 340 participants and 520 datasets. DAT, dopamine transporter; FDR, false discovery rate; GEE, generalized estimating equations; MixedLM, linear mixed-effects model; VentralDC, ventral diencephalon.

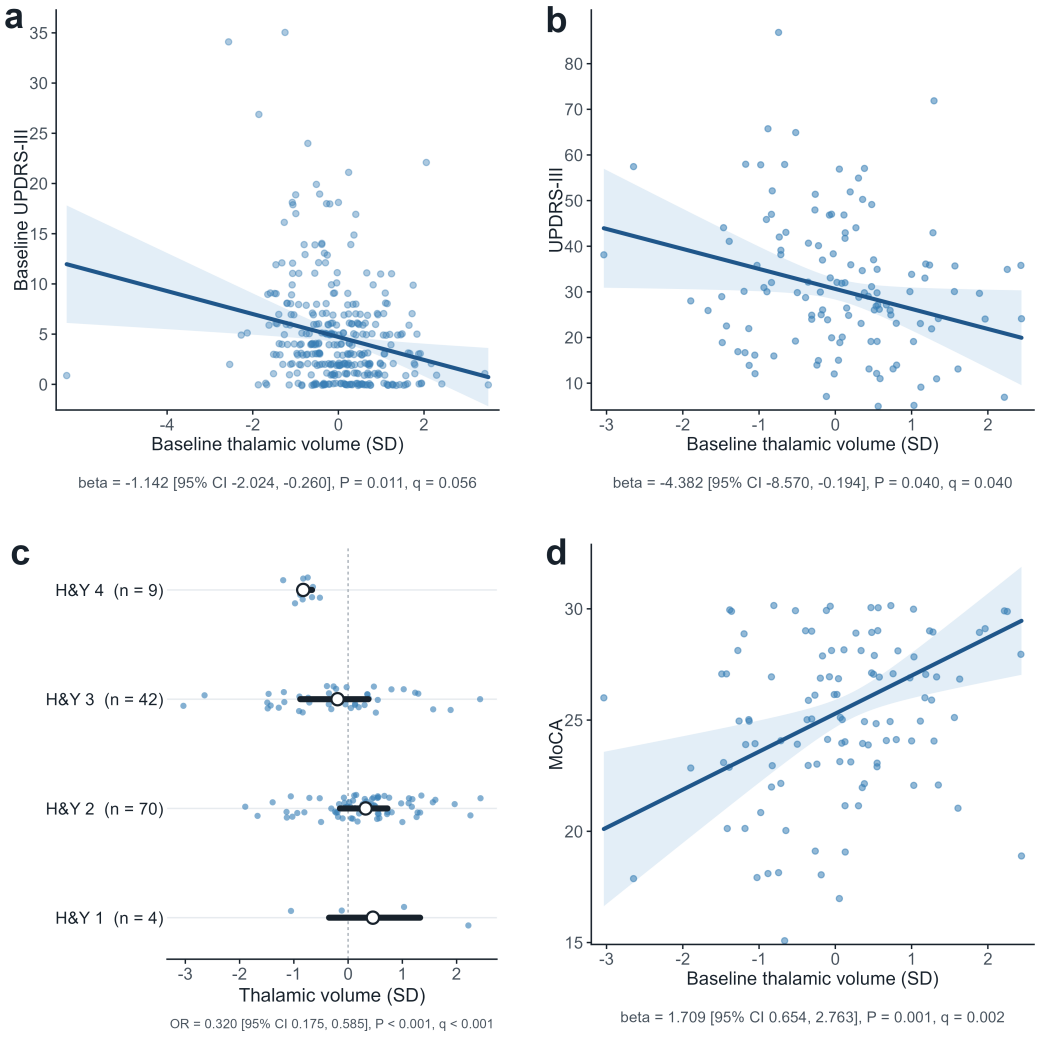

Figure 5: **Larger thalamic volume was associated with lower concurrent clinical burden. a,** Baseline whole-thalamus volume and UPDRS-III score in PPMI. Adjustment for age, sex, baseline DAT ratio and rapid eye movement sleep behavior disorder yielded $\beta = -1.142$ (95% confidence interval, -2.024 to -0.260; $P = 0.011$, $FDR = 0.056$; $n = 335$). **b,** Whole-thalamus volume and UPDRS-III score in QPN-NC. Adjustment for age, sex, estimated total intracranial volume and disease duration yielded $\beta = -4.382$ (-8.570 to -0.194; $P = 0.040$, $FDR = 0.040$; $n = 125$). **c,** Standardized whole-thalamus volume across Hoehn–Yahr stages in QPN-NC. Points, white circles and black lines show individual observations, medians and interquartile ranges; stage-specific sample sizes were 4, 70, 42 and 9. Adjusted proportional-odds regression yielded $OR = 0.320$ per 1-SD larger volume (0.175–0.585; $P < 0.001$, $FDR < 0.001$; $n = 125$). **d,** Whole-thalamus volume and MoCA score in QPN-NC. With the same adjustment as in **b**, $\beta = 1.709$ (0.654–2.763; $P = 0.001$, $FDR = 0.002$; $n = 110$). In **a**, **b** and **d**, points, solid lines and shading show individual observations, adjusted linear associations and 95% confidence intervals. Continuous outcomes used linear regression with heteroscedasticity-robust standard errors; the three QPN-NC outcomes were FDR-corrected as one family. DAT, dopamine transporter; FDR, false discovery rate; H&Y, Hoehn–Yahr; MoCA, Montreal Cognitive Assessment; OR, odds ratio; PPMI, Parkinson's Progression Markers Initiative; QPN-NC, Quebec Parkinson Network Neuroimaging Cohort; SD, standard deviation; UPDRS-III, Unified Parkinson's Disease Rating Scale Part III.

References

[1] Werner Poewe, Klaus Seppi, Caroline M. Tanner, Glenda M. Halliday, Patrik Brundin, Jens Volkmann, Anette-Eleonore Schrag, and Anthony E. Lang. Parkinson disease. *Nature Reviews Disease Primers*, 3(1):17013, 2017. doi: 10.1038/nrdp.2017.13.

[2] Bastiaan R Bloem, Michael S Okun, and Christine Klein. Parkinson's disease. *The Lancet*, 397 (10291):2284–2303, 2021. doi: 10.1016/s0140-6736(21)00218-x.

[3] Ronald B. Postuma, Daniela Berg, Matthew Stern, Werner Poewe, C. Warren Olanow, Wolfgang Oertel, José Obeso, Kenneth Marek, Irene Litvan, Anthony E. Lang, Glenda Halliday, Christopher G. Goetz, Thomas Gasser, Bruno Dubois, Piu Chan, Bastiaan R. Bloem, Charles H. Adler, and Günther Deuschl. Mds clinical diagnostic criteria for parkinson's disease. *Movement Disorders*, 30(12): 1591–1601, 2015. doi: 10.1002/mds.26424.

[4] Daniela Berg, Ronald B. Postuma, Charles H. Adler, Bastiaan R. Bloem, Piu Chan, Bruno Dubois, Thomas Gasser, Christopher G. Goetz, Glenda Halliday, Lawrence Joseph, Anthony E. Lang, Inga Liepelt-Scarfone, Irene Litvan, Kenneth Marek, José Obeso, Wolfgang Oertel, C. Warren Olanow, Werner Poewe, Matthew Stern, and Günther Deuschl. Mds research criteria for prodromal parkinson's disease. *Movement Disorders*, 30(12):1600–1611, 2015. doi: 10.1002/mds.26431.

[5] Sebastian Heinzel, Daniela Berg, Thomas Gasser, Honglei Chen, Chun Yao, and Ronald B. and Postuma. Update of the mds research criteria for prodromal parkinson's disease. *Movement Disorders*, 34(10):1464–1470, 2019. doi: 10.1002/mds.27802.

[6] Tanya Simuni, Lana M Chahine, Kathleen Poston, Michael Brumm, Teresa Buracchio, Michelle Campbell, Sohini Chowdhury, Christopher Coffey, Luis Concha-Marambio, Tien Dam, Peter DiBiaso, Tatiana Foroud, Mark Frasier, Caroline Gochanour, Danna Jennings, Karl Kieburtz, Catherine M Kopil, Kalpana Merchant, Brit Mollenhauer, Thomas Montine, Kelly Nudelman, Gennaro Pagano, John Seibyl, Todd Sherer, Andrew Singleton, Diane Stephenson, Matthew Stern, Claudio Soto, Caroline M Tanner, Eduardo Tolosa, Daniel Weintraub, Yuge Xiao, Andrew Siderowf, Billy Dunn, and Kenneth Marek. A biological definition of neuronal alpha-synuclein disease: towards an integrated staging system for research. *The Lancet Neurology*, 23(2):178–190, 2024. doi: 10.1016/s1474-4422(23)00405-2.

[7] Andrew Siderowf, Luis Concha-Marambio, D-E Lafontant, et al. Assessment of heterogeneity among participants in the parkinson's progression markers initiative cohort using alpha-synuclein seed amplification: a cross-sectional study. *The Lancet Neurology*, 22(5):407–417, 2023. doi: 10.1016/S1474-4422(23)00109-6.

[8] Valtteri Kaasinen and Tero Vahlberg. Striatal dopamine in parkinson disease: A meta-analysis of imaging studies. *Annals of Neurology*, 82(6):873–882, 2017. doi: 10.1002/ana.25103.

[9] G E Alexander, M R DeLong, and P L Strick. Parallel organization of functionally segregated circuits linking basal ganglia and cortex. *Annual Review of Neuroscience*, 9(1):357–381, 1986. doi: 10.1146/annurev.ne.09.030186.002041.

[10] Yoland Smith, Adriana Galvan, Tommas J. Ellender, Natalie Doig, Rosa M. Villalba, Icnelia Huerta-Ocampo, Thomas Wichmann, and J. Paul Bolam. The thalamostriatal system in normal and diseased states. *Frontiers in Systems Neuroscience*, 8:5, 2014. doi: 10.3389/fnsys.2014.00005.

[11] Anne-Caroline Martel and Adriana Galvan. Connectivity of the corticostriatal and thalamostriatal systems in normal and parkinsonian states: An update. *Neurobiology of Disease*, 174:105878, 2022. doi: 10.1016/j.nbd.2022.105878.

[12] Kirsten I. Taylor, Fabio Sambataro, Frank Boess, Alessandro Bertolino, and Juergen Dukart. Progressive decline in gray and white matter integrity in de novo parkinson's disease: An analysis of longitudinal parkinson progression markers initiative diffusion tensor imaging data. *Frontiers in Aging Neuroscience*, 10:318, 2018. doi: 10.3389/fnagi.2018.00318.

[13] Christina Tremblay, Nooshin Abbasi, Yashar Zeighami, Yvonne Yau, Mahsa Dadar, Shady Rahayel, and Alain Dagher. Sex effects on brain structure in de novo parkinson's disease: a multimodal neuroimaging study. *Brain*, 143(10):3052–3066, 2020. doi: 10.1093/brain/awaa234.

[14] Céline Charroud and Luca Turella. Subcortical grey matter changes associated with motor symptoms evaluated by the unified parkinson's disease rating scale (part iii): A longitudinal study in parkinson's disease. *NeuroImage: Clinical*, 31:102745, 2021. doi: 10.1016/j.nicl.2021.102745.

[15] Fatemeh Sadeghi, Abdullah Okar, Ronak Rashedi, Christian Gerloff, Dagmar Timmann, Robert Schulz, and Simone Zittel. Volumetric signatures of basal ganglia–thalamo–cortical and cerebello–thalamo–cortical networks in parkinson's disease and its motor subtypes. *Frontiers in Aging Neuroscience*, 18:1743479, 2026. doi: 10.3389/fnagi.2026.1743479.

[16] Daniele Caligiore, Rick C Helmich, Mark Hallett, Ahmed A Moustafa, Lars Timmermann, Ivan Toni, and Gianluca Baldassarre. Parkinson's disease as a system-level disorder. *npj Parkinson's Disease*, 2(1):16025, 2016. doi: 10.1038/npjparkd.2016.25.

[17] P.J. Planetta, E.T. Schulze, E.K. Geary, D.M. Corcos, J.G. Goldman, D.M. Little, and D.E. Vaillancourt. Thalamic projection fiber integrity in de novo parkinson disease. *American Journal of Neuroradiology*, 34(1):74–79, 2013. doi: 10.3174/ajnr.a3178.

[18] Conor Owens-Walton, David Jakabek, Brian D. Power, Mark Walterfang, Dennis Velakoulis, Danielle van Westen, Jeffrey C. L. Looi, Marnie Shaw, and Oskar Hansson. Increased functional connectivity of thalamic subdivisions in patients with parkinson's disease. *PLOS ONE*, 14(9): e0222002, 2019. doi: 10.1371/journal.pone.0222002.

[19] Jinse Park, Kang Min Park, Geunyeol Jo, Hyungon Lee, Byeong Sam Choi, Kyoung Jin Shin, Samyeol Ha, Seongho Park, Ho-joon Lee, and Hae Yu Kim. An investigation of thalamic nuclei volumes and the intrinsic thalamic structural network based on motor subtype in drug naïve patients with parkinson's disease. *Parkinsonism & Related Disorders*, 81:165–172, 2020. doi: 10.1016/j.parkreldis.2020.10.044.

[20] Juan Eugenio Iglesias, Ricardo Insausti, Garikoitz Lerma-Usabiaga, Martina Bocchetta, Koen Van Leemput, Douglas N. Greve, Andre van der Kouwe, Bruce Fischl, César Caballero-Gaudes, and Pedro M. Paz-Alonso. A probabilistic atlas of the human thalamic nuclei combining ex vivo mri and histology. *NeuroImage*, 183:314–326, 2018. doi: 10.1016/j.neuroimage.2018.08.012.

[21] Brendan Williams, Etienne Roesch, and Anastasia Christakou. Systematic validation of an automated thalamic parcellation technique using anatomical data at 3t. *NeuroImage*, 258:119340, 2022. doi: 10.1016/j.neuroimage.2022.119340.

[22] Brendan Williams, Dan Nguyen, Julie P. Vidal, and Manojkumar Saranathan. Thalamic nuclei segmentation from t1-weighted mri: Unifying and benchmarking state-of-the-art methods. *Imaging Neuroscience*, 2:1–16, 2024. doi: 10.1162/imag_a_00166.

[23] Vicente J. Ferrer-Gallardo, Teresa Esteban-Peñalba, Maria C. Rodriguez-Oroz, César Caballero-Gaudes, and Pedro M. Paz-Alonso. Thalamic nuclei volume changes associated with cognitive and motor manifestations of parkinson's disease. *npj Parkinson's Disease*, 11(1):279, 2025. doi: 10.1038/s41531-025-01129-2.

[24] Kenneth Marek, Danna Jennings, Shirley Lasch, Andrew Siderowf, Caroline Tanner, Tanya Simuni, Chris Coffey, Karl Kieburtz, Emily Flagg, Sohini Chowdhury, Werner Poewe, Brit Mollenhauer, Paracelsus-Elena Klinik, Todd Sherer, Mark Frasier, Claire Meunier, Alice Rudolph, Cindy Casaceli, John Seibyl, Susan Mendick, Norbert Schuff, Ying Zhang, Arthur Toga, Karen Crawford, Alison Ansbach, Pasquale De Blasio, Michele Piovella, John Trojanowski, Les Shaw, Andrew Singleton, Keith Hawkins, Jamie Eberling, Deborah Brooks, David Russell, Laura Leary, Stewart Factor, Barbara Sommerfeld, Penelope Hogarth, Emily Pighetti, Karen Williams, David Standaert, Stephanie Guthrie, Robert Hauser, Holly Delgado, Joseph Jankovic, Christine Hunter, Matthew Stern, Baochan Tran, Jim Leverenz, Marne Baca, Sam Frank, Cathi-Ann Thomas, Irene Richard, Cheryl Deeley, Linda Rees, Fabienne Sprenger, Elisabeth Lang, Holly Shill, Sanja Obradov, Hubert Fernandez, Adrienna Winters, Daniela Berg, Katharina Gauss, Douglas Galasko, Deborah Fontaine, Zoltan Mari, Melissa Gerstenhaber, David Brooks, Sophie Malloy, Paolo Barone, Katia Longo, Tom Comery, Bernard Ravina, Igor Grachev, Kim Gallagher, Michelle Collins, Katherine L. Widnell, Suzanne Ostrowizki, Paulo Fontoura, Tony Ho, Johan Luthman, Marcel van der Brug, Alastair D. Reith, and Peggy Taylor. The parkinson progression marker initiative (ppmi). *Progress in Neurobiology*, 95(4):629–635, 2011. doi: 10.1016/j.pneurobio.2011.09.005.

[25] Ziv Gan-Or, Trisha Rao, Etienne Leveille, Clotilde Degroot, Sylvain Chouinard, Francesca Cicchetti, Alain Dagher, Samir Das, Alex Desautels, Janelle Drouin-Ouellet, Thomas Durcan, Jean-François Gagnon, Angela Genge, Jason Karamchandani, Anne-Louise Lafontaine, Sonia Lai Wing Sun, Mélanie Langlois, Martin Levesque, Calvin Melmed, Michel Panisset, Martin Parent, Jean-Baptiste Poline, Ronald B. Postuma, Emmanuelle Pourcher, Guy A. Rouleau, Madeleine Sharp, Oury Monchi, Nicolas Dupré, and Edward A. Fon. The quebec parkinson network: A researcher-patient matching platform and multimodal biorepository. *Journal of Parkinson's Disease*, 10(1):301–313, 2020. doi: 10.3233/JPD-191775.

[26] Nikhil Bhagwat, Alain Dagher, and Jean-Baptiste Poline. Quebec parkinson network neuroimaging cohort (qpn-nc), 2025. URL https://doi.org/10.5281/zenodo.17246063. Dataset.

[27] Adriana Galvan, Annaelle Devergnas, and Thomas Wichmann. Alterations in neuronal activity in basal ganglia-thalamocortical circuits in the parkinsonian state. *Frontiers in Neuroanatomy*, 9:5, 2015. doi: 10.3389/fnana.2015.00005.

[28] Shuting Bu, Huize Pang, Xiaolu Li, Mengwan Zhao, Juzhou Wang, Yu Liu, Hongmei Yu, and Guoguang Fan. Structural and functional alterations of motor-thalamus in different motor subtype of parkinson's disease: An individual study. *Academic Radiology*, 31(4):1605–1614, 2024. doi: 10.1016/j.acra.2023.09.041.

[29] Yubing Chen, Zhiying Guo, Yajie Wang, Hangxing Yin, Shugang Zhang, and Weiguo Liu. Structural and functional differences of the thalamus between drug-naïve parkinson's disease motor subtypes. *Frontiers in Neurology*, 14:1102927, 2023. doi: 10.3389/fneur.2023.1102927.

[30] Bruce Fischl, David H. Salat, Evelina Busa, Marilyn Albert, Megan Dieterich, Christian Haselgrove, Andre van der Kouwe, Ron Killiany, David Kennedy, Shuna Klaveness, Albert Montillo, Nikos Makris, Bruce Rosen, and Anders M. Dale. Whole brain segmentation. *Neuron*, 33(3):341–355, 2002. doi: 10.1016/s0896-6273(02)00569-x.

[31] Bruce Fischl. Freesurfer. *NeuroImage*, 62(2):774–781, 2012. doi: 10.1016/j.neuroimage.2012.01.021.

[32] Ilkay Camlidag, Ersoy Kocabicak, Bunyamin Sahin, Ali Jahanshahi, Lutfi Incesu, Dursun Aygun, Onur Yildiz, Yasin Temel, and Umit Belet. Volumetric analysis of the subthalamic and red nuclei based on magnetic resonance imaging in patients with parkinson's disease. *International Journal of Neuroscience*, 124(4):291–295, 2014. doi: 10.3109/00207454.2013.843091.

[33] Javier Blesa, Inés Trigo-Damas, Michele Dileone, Natalia Lopez-Gonzalez del Rey, Ledia F. Hernandez, and José A. Obeso. Compensatory mechanisms in parkinson's disease: Circuits adaptations and role in disease modification. *Experimental Neurology*, 298:148–161, 2017. doi: 10.1016/j.expneurol.2017.10.002.

[34] Jinyoung Youn, Ji Hye Won, Mansu Kim, Junmo Kwon, Seung Hwan Moon, Minkyeong Kim, Jong Hyun Ahn, Jun Kyu Mun, Hyunjin Park, and Jin Whan Cho. Extra-basal ganglia brain structures are related to motor reserve in parkinson's disease. *Journal of Parkinson's Disease*, 13 (1):39–48, 2023. doi: 10.3233/JPD-223542.

[35] S. J. Palmer, J. Li, Z. J. Wang, and M. J. McKeown. Joint amplitude and connectivity compensatory mechanisms in parkinson's disease. *Neuroscience*, 166(4):1110–1118, 2010. doi: 10.1016/j.neuroscience.2010.01.012.

[36] Kristina Martinu and Oury Monchi. Cortico-basal ganglia and cortico-cerebellar circuits in parkinson's disease: Pathophysiology or compensation? *Behavioral Neuroscience*, 127(2):222–236, 2013. doi: 10.1037/a0031226.

[37] Linbo Wang, Ping Wu, Peter Brown, Wei Zhang, Fengtao Liu, Yan Han, Chuan-Tao Zuo, Wei Cheng, and Jianfeng Feng. Association of structural measurements of brain reserve with motor progression in patients with parkinson disease. *Neurology*, 99(10):e977–e988, 2022. doi: 10.1212/wnl.0000000000200814.

[38] Martin E Johansson, Ivan Toni, Bastiaan R Bloem, and Rick C Helmich. Parkinson's disease progression is shaped by longitudinal changes in cerebral compensation. *Brain*, 149(1):194–208, 2026. doi: 10.1093/brain/awaf302.

[39] Zhen Fan, Graham Searle, Gaia Rizzo, Justin Albani, Patrick Cella, Robert Comley, Gregory Klein, Luca Passamonti, Cristian Salinas, Adam J. Schwarz, Leonardo Iaccarino, Gilles Tamagnan, Jamie Eberling, Ken Marek, John Seibyl, Roger N. Gunn, and Parkinson's Progression Markers Initiative. Toward harmonizing quantification of dopamine neuron imaging biomarkers in parkinson's disease: The centamine scale. *Annals of Neurology*, 99(4):949–963, 2026. doi: 10.1002/ana.78116.